Biochemistry

Article

Cite This: Biochemistry 2019, 58, 4505−4518

pubs.acs.org/biochemistry

# Divalent Cations and the Divergence of βγ-Crystallin Function

Kyle W. Roskamp,[†] Natalia Kozlyuk,[†] Suvrajit Sengupta,[†] Jan C. Bierma,[‡] and Rachel W. Martin*[,†,‡]

[†]Department of Chemistry, University of California, Irvine, California 92697-2025, United States

[‡]Department of Molecular Biology and Biochemistry, University of California, Irvine, California 92697-3900, United States

Supporting Information

**ABSTRACT:** The βγ-crystallin superfamily contains both β- and γ-crystallins of the vertebrate eye lens and the microbial calcium-binding proteins, all of which are characterized by a common double-Greek key domain structure. The vertebrate βγ-crystallins are long-lived structural proteins that refract light onto the retina. In contrast, the microbial βγ-crystallins bind calcium ions. The βγ-crystallin from the tunicate *Ciona intestinalis* (*Ci*-βγ) provides a potential link between these two functions. It binds calcium with high affinity and is found in a light-sensitive sensory organ that is highly enriched in metal ions. Thus, *Ci*-βγ is valuable for investigating the evolution of the βγ-crystallin fold away from calcium binding and toward stability in the apo form as part of the vertebrate lens. Here, we investigate the effect of $Ca^{2+}$ and other divalent cations on the stability and aggregation propensity of *Ci*-βγ and human γS-crystallin (HγS). Beyond $Ca^{2+}$, *Ci*-βγ is capable of coordinating $Mg^{2+}$, $Sr^{2+}$, $Co^{2+}$, $Mn^{2+}$, $Ni^{2+}$, and $Zn^{2+}$, although only $Sr^{2+}$ is bound with comparable affinity to its preferred metal ion. The extent to which the tested divalent cations stabilize *Ci*-βγ structure correlates strongly with ionic radius. In contrast, none of the tested divalent cations improved the stability of HγS, and some of them induced aggregation. $Zn^{2+}$, $Ni^{2+}$, and $Co^{2+}$ induce aggregation by interacting with cysteine residues, whereas $Cu^{2+}$-mediated aggregation proceeds via a different binding site.

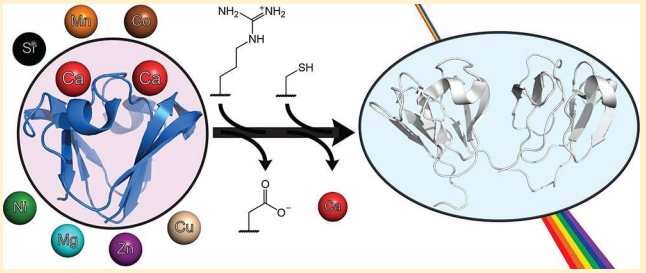


The vertebrate β- and γ-crystallins are structural proteins that make up the refractive tissue of the eye lens, where they compose up to 50% of the dry weight. Their extraordinary solubility enables them to pack at concentrations of >350 mg/mL in the lenses of humans and >750 mg/mL in those of fish. These strongly conserved proteins contain two or more βγ-crystallin domains, a β-sandwich structure comprising two sequential Greek key motifs, and are thought to share a common ancestor with the $Ca^{2+}$-binding βγ-crystallins found in microbes and invertebrates. Microbial βγ-crystallins contain a characteristic double-clamp $Ca^{2+}$-binding motif in which the loops situated atop the protein contribute binding residues to both sites. The idea that vertebrate lens crystallins evolved from calcium-binding βγ-crystallins, based on structural homology, is well supported in the literature on lens protein evolution.[1,2] The *Ci*-βγ crystallin from the tunicate *Ciona intestinalis* appears to bridge both crystallin functions. It is expressed in the papillae as well as the sensory vesicle, a structure found in ascidians that contains the gravity-sensing otolith and the light-sensitive ocellus.[3] A tunicate begins life as a free-swimming larva resembling a tadpole. During this larval stage, the animal navigates its environment using sensory inputs from the otolith and the ocellus.[4] Once it reaches the appropriate developmental stage, the tunicate attaches to a suitable substrate location via an adhesive secreted by the papillae.[5] The expression of *Ci*-βγ in both of these organs (and nowhere else)[6] underscores the significance of its dual role, representing a transition between the microbial calcium-binding crystallins and the vertebrate lens crystallins. *Ci*-βγ contains two functional double-clamp $Ca^{2+}$-binding sites and is also more highly refractive than its amino acid composition alone would suggest (although to a lesser extent than vertebrate lens proteins),[7] further suggesting dual functionality.

Despite their similar ancestry,[8,9] many of the vertebrate βγ-crystallins appear to have eschewed calcium binding activity,[10] possibly as a result of their evolution to the more stable two-domain structures, or simply through genetic drift.[11] Some reports have suggested that the lens β- and γ-crystallins weakly interact with calcium;[12,13] however, nuclear magnetic resonance (NMR) chemical shift perturbation suggests no structural changes upon addition of $Ca^{2+}$ for human γS-crystallin.[14] Moonlighting is seemingly omnipresent for vertebrate taxon-specific crystallins, including δ (argininosuccinate lyase),[15] ε (lactate dehydrogenase),[16] ζ (quinone reductase),[17] λ (3-hydroxyacyl-CoA dehydrogenase),[18] and τ (α-enolase),[19] as a variety of small, soluble proteins were recruited to the lens via gene duplication, raising the possibility that the ubiquitous vertebrate βγ-crystallins may have also retained cation-binding functionality.

The interactions of βγ-crystallins with divalent cations have important implications for lens homeostasis and cataractogenesis. For example, copper and zinc ions increase the chaperone activity of the lens α-crystallins but become displaced upon substrate binding.[20] Incubation of free zinc

**Received:** June 12, 2019
**Revised:** October 21, 2019
**Published:** October 24, 2019






DOI: 10.1021/acs.biochem.9b00507
Biochemistry 2019, 58, 4505−4518

and copper with γD-crystallin results in the formation of light scattering aggregates;[21,22] thus, a positive feedback cycle could exacerbate cataract formation. Moreover, elemental analysis of cataract and diabetic lenses has shown that elevated levels of copper are present.[23,24] Likewise, elevated levels of cadmium, iron, zinc, and other metals in cataracts have been reported by several groups.[25−27] An increased metal ion concentration in the lens could promote γ-crystallin aggregation directly[28] or indirectly through the displacement of copper from α-crystallins. In prion and other protein aggregation diseases, the displacement of copper alters protein−protein interactions and inhibits protein function.[29]

In contrast to the vertebrate γ-crystallins, which appear not to have significant cation interactions in the healthy lens, the cation-binding βγ-crystallins such as M-crystallin,[30] clostrillin,[31] rhodollin,[31] spherulin,[32] and protein S[33] exhibit dramatically increased thermal and chemical stability in the presence of calcium ions. These changes are often concomitant with binding-induced structural changes. The βγ-crystallin from *C. intestinalis* (*Ci-βγ*) is primarily found in the calcium carbonate-rich matrix of the otolith located above the photoreceptive ocellus. In addition to its location in a lens-like organ, the *Ci-βγ* gene promoter is functional in transgenic vertebrate assays, suggesting that it is a close homologue of the lens βγ-crystallins.[34] Unlike many other cation-binding βγ-crystallin domains, which are found within a higher-molecular weight protein, *Ci-βγ* has only a single domain. For these reasons, *Ci-βγ* is an ideal candidate for investigating differences in stability between the lens γ-crystallins and cation-binding βγ-crystallins.

In the $Ca^{2+}$-binding EF-hand motif of calmodulin[35] and ion channels,[36,37] other divalent cations may compete with $Ca^{2+}$ at its binding site. In fish otolith and lenses, environmentally common cations such as $Sr^{2+}$ and $Fe^{2+}$ are present in addition to trace metals, including $Mn^{2+}$, $Co^{2+}$, and $Pb^{2+}$.[38] The effect of non-calcium cation binding on the structure and stability of these proteins, however, remains incompletely characterized. Similarly, there has been limited research on the effect of non-oxidizing cations on lens βγ-crystallin interactions and stability. Understanding the similarities and differences between these crystallin subgroups beyond their overall structural fold is paramount to understanding the evolutionary development of lens protein stability. Moreover, a comparative analysis is also necessary for elucidating how exogenous factors influence βγ-crystallin behavior and to characterize the functional range of the crystallin double-clamp binding motif. To address these questions, we have investigated the effect of the divalent cations of magnesium, calcium, strontium, manganese, cobalt, nickel, zinc, and copper on the stability of human γS-crystallin (HγS) and *C. intestinalis* βγ-crystallin (*Ci-βγ*). We have also performed structural and sequence analysis of lens and cation-binding βγ-crystallins to place these experimental observations in an evolutionary context.

## MATERIALS AND METHODS

**Amino Acid Composition Analysis.** The DNA sequences of lens γ-crystallins were collected from NCBI (https://www.ncbi.nlm.nih.gov/protein) searches using the keywords "gamma crystallin", "beta crystallin S", "beta gamma crystallin", and "betagamma crystallin" and filtered for "Animals" and sequences between 170 and 185 residues. Low-quality, crystallin-like, homologue, related, point mutant, partial, and incomplete sequences were removed by manual review of each entry. Leading methionine residues were removed from applicable sequences. To avoid overweighting, only one paralog of polymorphic γ-crystallins was used in the final data set. To maintain the similarity to the experimentally characterized human γS-crystallin, only γ-crystallin sequences from terrestrial vertebrates were analyzed. The final data set was composed of 50 γA-, 78 γB-, 62 γC-, 55 γD-, and 62 γS-crystallins. Additionally, the DNA sequences corresponding to the seven βγ-crystallin proteins for which Protein Data Bank (PDB) structures confirm cation-binding coordination through the double-clamp binding motif (PDB entries 1HDF,[39] 1NPS,[33] 2BV2,[6] 3HZB,[31] 3HZ2,[31] 3I9H,[31] and 4IAU[40]) were collected from the NCBI database. γE-, γF-, and γN-crystallins were excluded from this study because they are not expressed or are pseudogenes in humans.

**Sequence Alignments and Selection Analysis.** The alignments for all DNA and protein sequences were generated using MEGA7.[41] Protein sequences were aligned using MUSCLE with default gap penalties and the UPGMB clustering matrix.[42] Trees for each alignment were then constructed from the DNA of the aligned protein sequences using the neighbor-joining method. Preliminary d*N*/d*S* calculations for selection at each codon were subsequently calculated using Felsenstein 1981 (F1981), General Time Reversible (GTR), Hasegawa−Kishino−Yano (HKY), and Tamura−Nei (TN) methods from MEGA7. Further codon selection analysis was also calculated using the methods of single-likelihood ancestor counting (SLAC) and fixed effects likelihood (FEL) using HyPhy,[43] which produced identical results.

**Solvent-Exposed Surface Area.** The side chain solvent-accessible surface area (SASA) for cysteine residues was calculated using VADAR (http://vadar.wishartlab.com/).[44] Structures from the PDB were used for γB (PDB entry 2JDF[45]), γC (PDB entry 2NBR[46]), γD (PDB entry 1HK0[47]), and γS (PDB entry 2M3T[48]), whereas an ITASSER model[49] was generated for γA, for which no experimental structure was available.

**Protein Expression and Purification.** Expression and purification of natural abundance and uniformly $^{15}N$-labeled tunicate βγ-crystallin and human γS-crystallin were performed as previously described.[14] Briefly, the genes encoding each protein were cloned into a pET28a(+) vector (Novagen, Darmstadt, Germany) and overexpressed in a Rosetta *Escherichia coli* cell line (DE3) using Studier's autoinduction protocol.[50] Tunicate βγ-crystallin lysate was purified via anion exchange and two runs of size-exclusion chromatography. Human γS-crystallin[a] with an N-terminal six-His tag and a TEV cleavage sequence (ENLFQG) was purified via nickel affinity chromatography, digestion with TEV protease (produced in house), subsequent nickel affinity chromatography, and, finally, two size-exclusion chromatography (SEC) runs. The monomeric and dimeric species were collected separately from the first SEC purification and then subjected to SEC a second time. All samples were dialyzed into metal-free 10 mM HEPES and 0.05% $NaN_3$ (pH 7.1) unless otherwise stated. Similarly, all samples were reduced via incubation with 5 mM dithiothreitol (DTT) (made fresh) for 30 min at room temperature, dialyzed overnight to remove DTT, and used for measurements immediately thereafter. This procedure was used to prevent the spontaneous dimer formation that can occur at higher concentrations in the absence of a reducing agent.[51]



DOI: 10.1021/acs.biochem.9b00507
*Biochemistry* 2019, 58, 4505−4518

**Turbidity (light scattering).** A Spark TECAN plate reader (Tecan Trading AG) was used to measure light scattering (405 nm) of *Ci-βγ*, HγS-WT, and HγS variants in the presence of $Cu^{2+}$ and $Zn^{2+}$ at 30 °C and $Co^{2+}$ and $Ni^{2+}$ at 42 °C; 200 μL of protein at 50 μM [10 mM HEPES and 50 mM NaCl (pH 7.1)] was placed in a 96-well plate and treated with variable equivalents of divalent cation after a 5 min baseline period. In $Zn^{2+}$ measurements, after 2 h, 2, 10, or 20 equiv (10 μL) of ethylenediaminetetraacetic acid (EDTA) was added to the solution to chelate available cations. Measurements were recorded every 60 s with 5 s of shaking before readings. The reported measurements were determined by subtracting the absorbance of the buffer measured in parallel. The light scattering observed for the protein-only solution was identical to that of the buffer-only samples and has been omitted for the sake of clarity. To minimize potential instrumental bias, the locations of all samples on a plate were assigned at random.

**Tryptophan Fluorescence.** Thermal denaturation was detected via intrinsic tryptophan fluorescence for *Ci-βγ* and HγS-WT. Five micromolar protein solutions with 50 μM divalent cation ($CaCl_2$, $CoCl_2$, $MgCl_2$, $MnCl_2$, $NiCl_2$, $SrCl_2$, or $ZnCl_2$) or EDTA added were assayed incrementally over a 17−99 °C temperature range. Measurements were taken using a Varian Cary Eclipse fluorescence spectrophotometer with an excitation wavelength of 280 nm and a 5 nm excitation slit. The sample temperatures were controlled using a Quantum Northwest TC 1 temperature controller (Quantum Northwest, Inc.) with a 2 min equilibration at each 1 °C temperature increment. The fraction unfolded was calculated from the 360 nm/320 nm fluorescence ratio and fit to a two-state equilibrium unfolding model to determine the denaturation midpoint temperature ($T_m$) of each sample. Fluorescence changes at 330 nm were calculated by subtracting the native protein fluorescence of each sample from the fluorescence following divalent cation addition. Samples were allowed to thermally equilibrate to within instrument sensitivity at 20 °C for 2 min before measurements were taken.

The change in intrinsic tryptophan fluorescence was measured for each aforementioned divalent cation. A 1000 μL sample containing 5 μM protein was measured prior to and following the addition of 10 μL of 5 mM divalent cation. Measurements were repeated six times for each divalent cation.

**Dynamic Light Scattering.** Thermal gradient dynamic light scattering (DLS) measurements were performed using a Malvern Zetasizer NS for *Ci-βγ* measurements and a Malvern Zetasizer μV for HγS measurements. Each sample was composed of 150 μM protein with 975 μM divalent cation. Experiments were performed at 1 °C increments from 20 to 92 °C with 2 min equilibrations before measurements and 1 °C/min temperature ramping between measurements. Ten second correlations were measured six times and repeated three times for each temperature step.

**Mass Spectrometry.** The insoluble aggregates of HγS-WT and HγS-$C_0$ with 10 equiv of $CuCl_2$ were prepared via incubation at 30 °C for 12 h and collected via centrifugation. Pellets were washed four times with doubly deionized water, once with 20 equiv of EDTA, once with 10 mM DTT, and twice more with doubly deionized water. The samples were then dialyzed into doubly deionized water to remove urea; 0.5 mg/mL samples of both proteins were digested using MS grade Pierce Trypsin Protease (ThermoFischer Scientific, Rockford, IL) with or without DTT at 37 °C overnight. A Waters Synapt G2 mass spectrometer was used to detect the resulting peptide fragments with a 30 min separation on a Waters I-Class UPLC column. The resulting MS and MS/MS data were analyzed using BioPharmaLynx for peptide and post-translational modification (PTM) identification. HγS-WT and HγS-$C_1$ digests were analyzed for only cysteine oxidation products. HγS-$C_0$ and *Ci-βγ* were probed for PTMs. The following PTMs were sought on the basis of previously observed modifications in aged and cataractous lenses[52,53] and known radical oxidative products:[54,55] −18 Da [dehydration/succinimide (S, T/N, D)], +1 Da [deamidation (N, D) or 2-amino-3-oxo-butanoic acid (T)], +4 Da [kynurenine (W)], +16 Da [oxidation/hydroxylation (M, C, H, W, F, Y, N, D)], +28 Da [carbonylation (S, H, K)], +32 Da [dioxidation (C, M)], and +55 Da (R). Missed trypsin cleavages were required for modified arginine or lysine residues. Only peptides in which at least 35% of b and y ions were observed for the parent and modified fragments were considered.

**Isothermal Titration Calorimetry (ITC).** ITC measurements were performed using a MicroCal PEAQ-ITC instrument (Malvern Instruments, Northampton, MA). Each titration consisted of 1.5 μL injections of a 2 mM ($Ca_2$ or $SrCl_2$) or 5 mM ($Mg_2$, $Mn_2$, $Co_2$, $Ni_2$, or $Zn_2$) cation solution to a 200 μM protein sample in 10 mM HEPES (pH 7). Injections were made every 180 s for $CaCl_2$ and $SrCl_2$. The remaining samples had the initial 10 injections made every 300 s and every 200 s for the remaining injection. In total, 25 titrations were performed. To control for the heat of dilution, 10 mM divalent cation was titrated into 10 mM HEPES and the resulting data were subtracted from the raw protein data. The ITC data were initially analyzed using Mathematica as previously described[14] to obtain reasonable initial values and then fit to a two-state binding model using MicroCal PEAQ-ITC Analysis Software. The reported fit parameters are the mean of two trials, while the error bars represent one standard deviation.

**Solution-State NMR Spectroscopy.** Experiments were performed at 25 °C on a Varian $^{Unity}$INOVA system operating at an 800 MHz proton Larmor frequency and equipped with a $^1H/^{13}C/^{15}N$ 5 mm triaxis PFG triple-resonance probe. $^{15}N-^1H$ HSQC experiments were acquired with four scans in the direct dimension and 64 scans in the indirect dimension at protein concentrations of 1.7 mM in the presence of 1, 2, and 6.5 equiv of $MgCl_2$, $NiCl_2$, $ZnCl_2$, or $SrCl_2$.

Chemical shift perturbations (CSP) were calculated using the equation $\Delta\delta_{avg} = \sqrt{\frac{(\Delta\delta_N / 5)^2 + (\Delta\delta_H)^2}{2}}$. Chemical shift perturbation thresholds for strong (CSP ≥ 0.2 ppm) and moderate (0.2 ppm > CSP ≥ 0.06 ppm) were based on the chemical shift perturbation reported previously for interactions of *Ci-βγ* with $Ca^{2+}$.[14] A CSP of <0.06 ppm was classified as unperturbed.

**Far-Ultraviolet (far-UV) Circular Dichroism.** The far-UV circular dichroism (CD) spectra of 5 μM HγS were recorded on a J-810 spectropolarimeter (JASCO, Easton, MD). Spectra were recorded from 250 to 195 nm using a 1 nm bandwidth and 4 s response.

## RESULTS AND DISCUSSION

**Vertebrate Lens and Cation-Binding βγ-Crystallins Differ in Amino Acid Composition.** Irrespective of function, all βγ-crystallins are topologically similar. One important conserved feature is an (F/Y/W)xxxx(F/Y)xG



DOI: 10.1021/acs.biochem.9b00507
*Biochemistry* 2019, 58, 4505−4518

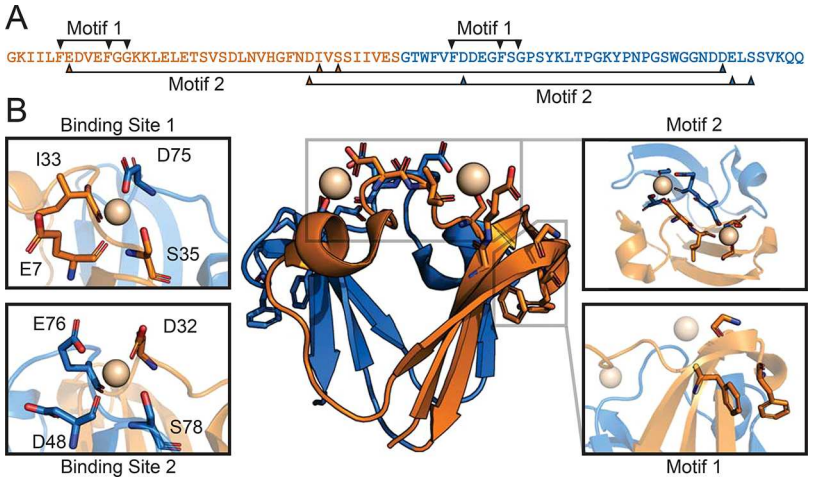


**Figure 1.** (A) Sequence of *Ci-βγ* annotated with the residues comprising the (F/Y/W)xxxx(F/Y)xG (motif 1) and cation-binding site (motif 2). The residues of the first Greek key are colored orange; those of the second Greek key are colored blue. (B) Both motifs are visualized within the calcium-bound X-ray crystal structure of *Ci-βγ* (PDB entry 2BV2).[6] Secondary images are displayed on the right for the sake of clarity. The residues comprising the first and second binding site are displayed to the left. The first binding site consists of the D75 side chain carboxylate, the S35 side chain hydroxyl, the E7 backbone carbonyl, and the I33 backbone carbonyl. The second binding site consists of the D32 side chain acid, the S78 side chain hydroxyl, the E48 backbone carbonyl, the E76 backbone carbonyl, and the E76 side chain carboxylate.

motif in the first two *β*-strands of each Greek key (Figure 1). Additionally, disabled versions of the (N/D)(N/D)xx(T/S)S $Ca^{2+}$ sequence characteristic of cation-binding *βγ*-crystallins are readily evident in vertebrate lens *γ*-crystallins. Point mutations in either motif can compromise protein solubility and result in cataract.[56−60] In particular, reintroduction of $Ca^{2+}$ binding ability in lens *γ*-crystallins decreases protein stability,[2,61,62] raising questions about how vertebrate lens proteins evolved from their metal-binding ancestors. To assess the conservation of residues associated with divalent cation binding during crystallin evolution, the amino acid sequences of cation-binding *βγ*-crystallins were compared to those of terrestrial vertebrate lens γA-, B-, C-, D-, and S-crystallins. For this analysis, γA−D-crystallins were clustered together on the basis of known similarities in gene structure, conservation, and sequence,[63,64] while γS-crystallins were analyzed separately.

One notable difference between the lens and cation-binding *βγ*-crystallins is in the numbers of positively and negatively charged residues. Cation-binding *βγ*-crystallins have a net negative charge to aid in the sequestration of cations. In particular, *Ci-βγ* lacks positively charged residues in the vicinity of the $Ca^{2+}$-binding sites; however, this feature is not strongly conserved among other cation-binding *βγ*-crystallins. The lens *γ*-crystallins contain similar levels of positively and negatively charged residues, with charged residues evenly dispersed across the protein's surface. On average, lens *γ*-crystallins contain similar total levels of arginine and lysine (γA−D, 12.9 ± 0.8%; γS, 12.4 ± 0.8%), histidine (γA−D, 3.2 ± 1.0%; γS, 3.2 ± 0.8%), and acidic residues (γA−D, 12.8 ± 0.6%; γS, 13.5 ± 0.4%) (Figure 2 and Table S1). Cation-binding *βγ*-crystallins contain comparable levels of negatively charged residues (*βγ*, 11.5 ± 2.6%) but lower levels of arginine and lysine residues (*βγ*, 8.2 ± 2.5%). Similarly, low levels of histidine (0.7 ± 0.6%), cysteine (0.5 ± 0.9%), and methionine (0.6 ± 0.9%) are found in the cation-binding crystallins. This observation is unsurprising, as cysteine and histidine are the most commonly observed residues in protein metal-binding sites and are therefore expected to be localized to the binding sites and hence rare overall.[65] Furthermore, cysteine and methionine can

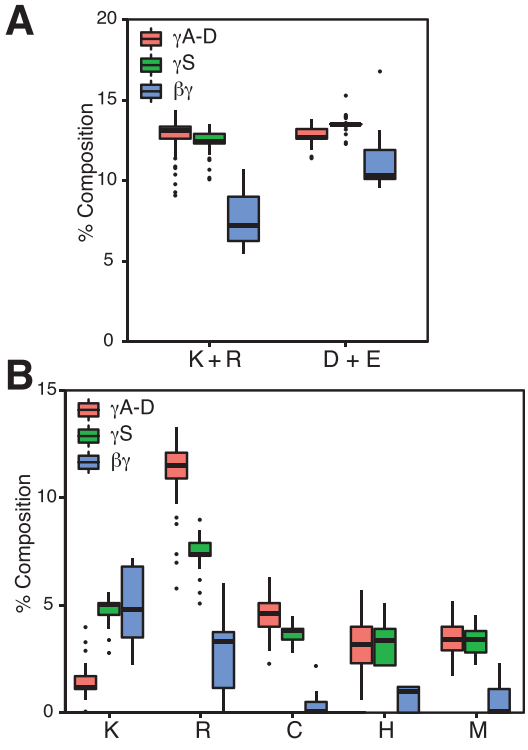


**Figure 2.** Combined and individual amino acid sequence percentages of lens γA−D (red), lens γS (green), and cation-binding *βγ*-crystallins (blue). Each box covers the 25th to 75th percentiles, and whiskers extend to 1.5 times the largest value in the respective quartile range. (A) Percentages of positively charged (lysine and arginine) and negatively charged (aspartate and glutamate) residues. (B) Lysine, arginine, cysteine, histidine, and methionine sequence percentage of each group.

be readily oxidized. Post-translational modifications at these sites could result in structural changes, either decreasing the stability of the apo form or the binding affinity in the holo form. Despite their similar net charges, the γA−D- and γS-crystallins differ substantially in the distribution of positively



DOI: 10.1021/acs.biochem.9b00507
*Biochemistry* 2019, 58, 4505−4518

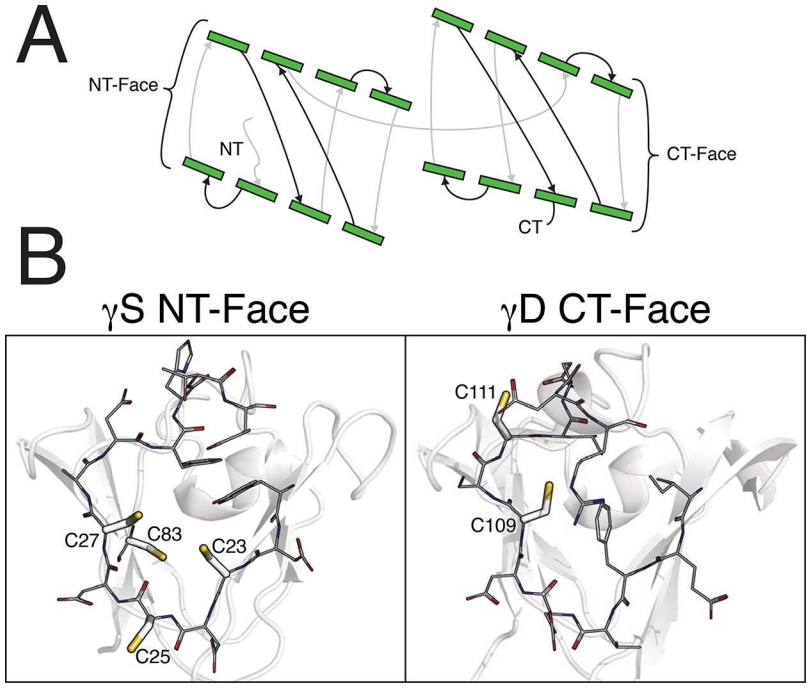


**Figure 3.** (A) Schematic of the γ-Crystallin structure showing the location of the external β-sandwich faces of the N-terminal and C-terminal domains. The β-strands of the protein are shown as green rectangle lines drawn between them to illustrate the relative strand connectivity (black, top; gray, bottom). (B) Ribbon structure of the N-terminal face of γS (PDB entry 2M3T[48]) and the C-terminal face of γD-crystallin (PDB entry 1HK0[47]) overlaid with line renderings of relevant residues. The cysteines of both faces are shown as sticks. γS-C83 is depicted in the γS-NT face due to its proximity despite being located one β-strand behind the N-terminal face.

charged residues between lysine and arginine. On average, γA−D-crystallins have a 17:2 arginine:lysine ratio compared to the 3:2 ratio observed in the γS-crystallins. This difference may be driven in part by the higher refractivity of arginine, as γA−D-crystallins are located in the more highly refractive lens nucleus, while γS-crystallins are more abundant in the cortex.[66]

**Solvent-Exposed Cysteines Are Strongly Conserved in Lens Crystallins but Not Calcium-Binding Crystallins.** Methionine, cysteine, and histidine are more common in lens γ-crystallins than in calcium-binding crystallins, consistent with their high refractivity. Methionine is particularly abundant in fish γM-crystallins, many of which contain ≤15% methionine.[67] Overall, the refractive function of lens proteins leads to their being enriched in polarizable amino acids.[68] Here, both groups of lens γ-crystallins are enriched in highly refractive amino acids relative to their metal-binding counterparts (Figure S1), consistent with the measured difference in d*n*/d*c* values for human γS (0.2073) and *Ci*-*βγ* (0.1985).[7] Relative to side chain size, cysteine is the most refractive whereas alanine is the least refractive of any amino acid (Figure S2), leading to the hypothesis that cysteine plays a critical functional role in the highly refractive lens crystallins. This idea is supported by the sequence data, which indicate that many cysteine residues found in lens γ-crystallins are replaced by other residues in cation-binding crystallins (Table S2). In contrast to cation-binding *βγ*-crystallins, where the few cysteines present are usually found in disulfide bonds, lens proteins have free, solvent-exposed cysteines (Tables S3 and S4) whose function is not fully understood. Although serine is the most common alternate residue at consensus cysteine positions, a variety of amino acids are observed at the homologous positions in other γ-crystallins (Table S2).

In lens γ-crystallins, several conserved cysteine positions are found, predominately in the N-terminal domain (Table S5). For both domains, the cysteines closest to one another in space are located in and around the third β-strand. The most concentrated locus of conserved cysteines is found in the N-terminal domain of HγS. C23 and C27 make up the closest cysteine pair in this region and are both spatially adjacent to C25 and C83 (Figure 3). The location of C23, C25, and C27 across the second and third β-strands of the first Greek key results in high solvent accessibility (21%, 77%, and 40%, respectively) for each side chain. Both of these features, proximity and high solvent accessibility, were noted by Thorn et al. as factors enabling this triad to drive the formation of domain-swapped dimers.[51] Across the lens γA−D-crystallins, the positions homologous to C23 and C83 are similarly occupied by cysteines. The position homologous to C27 is the most conserved position across both domains of the lens γ-crystallins and is replaced by a histidine only in the N-terminal domain of γD, while the C25 position is unique to the γS-crystallins.

The apparent functional significance of these conserved cysteine residues raises questions about the underlying selection process. Although these residues are highly refractive, they are also capable of non-native intermolecular disulfide bond formation that can lead to aggregation, complicating their utility in an environment where solubility is just as critical as refractivity. Disulfide exchange in human lens γ-crystallins has recently been proposed to help regulate the local redox potential of the lens;[69] however, inter- and intramolecular disulfide bonding has also been shown to facilitate domain swapping in γS-crystallin, providing a possible nucleation site for the formation of deleterious aggregates.[51] Cysteines from each γ-crystallin have also been identified as sites for post-


DOI: 10.1021/acs.biochem.9b00507
*Biochemistry* 2019, 58, 4505−4518

Table 1. Thermodynamic Parameters for Binding of $Ca^{2+}$ and $Sr^{2+}$ to *Ci-βγ*

| | $K$ ($M^{-1}$) | $\Delta H$ (kJ/mol) | $\Delta G$ (kJ/mol) | $-T\Delta S$ (kJ/mol) |
|---|---|---|---|---|
| $Ca^{2+}$ site 1 | $(3.5 \pm 2.2) \times 10^8$ | −26.6 ± 6.5 | −48.5 ± 1.7 | −21.9 ± 8.7 |
| $Ca^{2+}$ site 2 | $(5.9 \pm 1.2) \times 10^7$ | −21.9 ± 0.8 | −44.4 ± 0.5 | −22.5 ± 0.3 |
| $Sr^{2+}$ site 1 | $1.2 \times 10^8 \pm 1.8 \times 10^7$ | −31.6 ± 2.3 | −46.0 ± 0.4 | −14.4 ± 2.5 |
| $Sr^{2+}$ site 2 | $(5.6 \pm 3.2) \times 10^6$ | −18.5 ± 1.7 | −38.3 ± 1.6 | −19.8 ± 3.3 |

translational modifications in aged lenses,[52,70] while the more solvent-exposed cysteines of γD-crystallin have been shown to be the primary contributors to copper-mediated aggregation.[22]

For all conserved cysteine positions, we calculated the nonsynonymous and synonymous codon substitutions to investigate potential selective pressure. For each γ sequence alignment, a maximum-likelihood phylogenetic reconstruction was performed to enable calculation of the nonsynonymous and synonymous substitution rates via SLAC (single-likelihood ancestor counting) and FEL (fixed effects likelihood).[71] No positions exhibit evidence of positive (diversifying) selection, while numerous cysteines, particularly in γS-crystallin, exhibit evidence of strong negative (purifying) selection. Compared to the α- and β-crystallins, the γ-crystallins are the most enriched with cysteine. Moreover, in the six human β-crystallins, a cysteine is observed at the position homologous to C27 in HγS, with only 15 total cysteines elsewhere. Notably, no substitutions were observed for the codons of γA-C78, γC-C108 (human γD numbering convention), and γS-C83 (human γS numbering convention). No evidence of positive selection was observed for any of the sites examined across all lens γ-crystallins. Each of the seven conserved cysteines of the γS-crystallins appears to experience strong negative selection ($p \leq 0.05$), while ∼20% of γA−D-crystallins experience similar selection (Table S6).

The high level of conservation of cysteines in all γ-crystallin sequences and the mutual proximity of the cysteines in the N-terminal domain of γS-crystallin led us to design variants that remove one or more prominently exposed Cys residues in HγS. We hypothesize that if divalent cation interactions are relevant to protein stability or lens homeostasis, mutating C23, C25, and/or C27 would alter cation-binding activity. Therefore, variants with two (HγS-$C_2$ = γS-C23S/C27S), one (HγS-$C_1$ = γS-C23S/C25S/C27S), or zero (HγS-$C_0$ = γS-C23S/C25S/C27S/C115S) solvent-accessible cysteines were produced. For each mutation, we chose serine, as opposed to alanine, as a replacement due to its similar size and the observation that it is the most common alternative residue at these sites. The resulting variants also enabled us to more directly compare the behavior of human γS-crystallin and *Ci-βγ*, which does not contain cysteine, in the presence of various divalent cations. The results of these experiments are described in subsequent sections.

***Ci-βγ* Can Accommodate a Wide Range of Divalent Cations.** Unlike better-characterized $Ca^{2+}$ motifs, such as the EF-hand[72,73] or C2 domain,[74] the double-clamp motif of βγ-crystallins has not yet been thoroughly tested for non-$Ca^{2+}$ divalent cation interactions. Previous research has shown Protein S binds $Mg^{2+}$ with an affinity that is 1 order of magnitude lower,[75] and M-Crystallin has been crystallized in the presence of $Mg^{2+}$ (PDB entry 5HT9); however, neither domain of *Yersinia* crystallin interacts with $Mg^{2+}$.[76] *Ci-βγ* is a useful βγ-crystallin for investigating non-$Ca^{2+}$ divalent cation binding, due to its high $Ca^{2+}$ affinity, its native monomeric form, and the minor asymmetry between its binding sites. Moreover, its native location in a light-sensing organ makes it the best cation-binding βγ-crystallin for comparative analysis with lens γ-crystallins. *Ci-βγ* binds $Ca^{2+}$ via two-site sequential binding, with high affinity at both sites relative to those of other βγ-crystallins.[14,62]

Here, we used isothermal titration calorimetry (ITC) to investigate the thermodynamics of interactions between *Ci-βγ* and a variety of divalent cations. The binding isotherms for binding of *Ci-βγ* to $Ca^{2+}$ and $Sr^{2+}$ were exothermic, while the rest exhibited biphasic behavior. Similar results have been previously reproted for other systems, e.g., refs 77−79. The extent of exothermic character of the biphasic isotherms decreased in the following order: $Mg^{2+}$ > $Mn^{2+}$ > $Co^{2+}$ > $Ni^{2+}$ > $Zn^{2+}$ (Figure S3). The isotherm produced by $Sr^{2+}$ was highly similar to that of $Ca^{2+}$; the observed data for both cases could be fit to same exothermic two-state model previously reported[14] (Figure S4). The binding constants and parameters calculated show slightly stronger binding than we previously reported for *Ci-βγ* to $Ca^{2+}$ in Tris buffer. The overall dissociation constant $[K_d = 1/\sqrt{(K_1K_2)}]$ for $Ca^{2+}$ was found to be 0.004 μM, that for $Sr^{2+}$ 0.039 μM (Table 1).[14] The identities of the binding sites corresponding to the high- and lower-affinity binding of $Ca^{2+}$ and $Sr^{2+}$ are not yet known; however, we suspect the higher-affinity binding of both cations occurs at the five-coordinate site and the lower-affinity binding occurs at the four-coordinate site. The two sites are nearly identical, differing only in their third residues. In the first binding site, I33 coordinates cations via its backbone carbonyl whereas the homologous E76 at the second site also coordinates through its side chain (Figure 1). The side chain coordination from the third residue of the second binding site in *Ci-βγ* is not observed in any other cation-binding βγ-crystallin, which may explain the remarkably high $Ca^{2+}$ affinity of this protein.

*Ci-βγ* and M-crystallin (36.6% identical and 67.1% similar as determined via LALIGN[80]) both exhibit similar structural changes upon $Ca^{2+}$ binding, contain two octahedral binding sites, and bind via two-site sequential binding with a 1 order of magnitude difference between sites.[30] A comparison of M-crystallin crystal structures bound to $Ca^{2+}$ (PDB entry 3HZ2[31]) and $Mg^{2+}$ (PDB entry 5HT9) shows that the ligand−cation distances are shorter for $Mg^{2+}$ binding (Table S7). The tetrahedral volume between binding site ligands decreases more at the second site from $Ca^{2+}$ and $Mg^{2+}$ binding. The greater reduction in ligand space suggests a greater flexibility at the second binding site. We hypothesize that the second site of *Ci-βγ* is similarly flexible and would therefore bind with a higher affinity.

Residue-specific interactions of $Sr^{2+}$, $Mg^{2+}$, $Ni^{2+}$, and $Zn^{2+}$ with *Ci-βγ* were investigated using solution-state NMR. $^1H-^{15}N$ HSQC[81] chemical shift perturbations (CSPs) were measured to identify the residues involved in divalent cation interactions (Figures S5 and S6). Classification of CSP strength was done according to standard threshold levels (strong, ≥0.2; moderate, ≥0.06). Strong and moderate CSPs



DOI: 10.1021/acs.biochem.9b00507
*Biochemistry* 2019, 58, 4505−4518

from the addition of 6.5 equiv of divalent cation are shown mapped onto the X-ray crystal structures of the $Ca^{2+}$-bound protein (PDB entry 2BV2)[6] in Figure 4. The regions

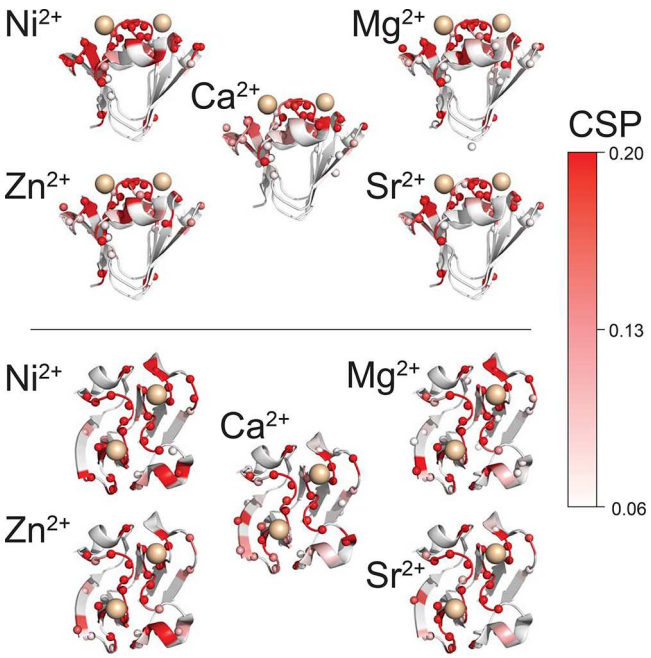


**Figure 4.** $^{1}H-^{15}N$ HSQC CSPs of *Ci-βγ* resulting from the addition of 6.5 equiv of $Ca^{2+}$, $Sr^{2+}$, $Mg^{2+}$, $Ni^{2+}$, and $Zn^{2+}$ were mapped onto the structure of *Ci-βγ* (PDB entry 2BV2). Weak CSPs (≤0.06) are colored white, strong CSPs (≥0.2) red, and moderate CSPs from red to white. The color gradient is projected onto the backbone and the spheres representing backbone amide nitrogens. $Ca^{2+}$ ions found in the crystal structure are represented as tan spheres.

corresponding to strong CSPs and absent peaks resulting from $Sr^{2+}$, $Mg^{2+}$, $Ni^{2+}$, and $Zn^{2+}$ interactions exhibited distributions that strongly resemble the CSP profile of $Ca^{2+}$-bound *Ci-βγ*.

For all of the divalent cation interactions, strong CSPs were concentrated in the loop regions (31−36 and 72−79) containing three of the four binding moieties for each site (site 1, I33-O, S35-OG, and D75-OD1; site 2, D32-OD1, E76-O/OE1, and S78-OG). The residues completing the binding site motifs (site 1, E7-O/OE1; site 2, D42-O), located before the *β*-hairpins, also displayed moderate to strong CSPs. Minor CSPs were also observed along the *β*-strands of the Greek keys and in other solvent-exposed surfaces away from the two binding sites for all divalent cations. Notably, above 3 equiv of metal cation, $Ni^{2+}$ binding resulted in the disappearance of chemical shifts from residues at and adjacent to the calcuim-binding site, presumably due to paramagnetic relaxation enhancement, whereas $Zn^{2+}$, and to a lesser extent $Mg^{2+}$, yielded fewer assignable chemical shifts, possibly due to a transition into the intermediate exchange dynamic regime. In general, each tested metal cation interacts strongly with residues composing and adjacent to the $Ca^{2+}$-binding site. Although the ability of $Mg^{2+}$, $Sr^{2+}$, and various transition metals to coordinate to $Ca^{2+}$-binding sites has been reported for other $Ca^{2+}$-binding proteins such as calmodulin,[82−84] calcium- and integrin-binding protein,[85,86] and parvalbumin,[87] this represents the first demonstration of a *βγ*-crystallin coordinating a wide range of non-$Ca^{2+}$ cations.

**Divalent Cations Increase the Thermal Stability of *Ci-βγ* but Not That of HγS.** Biophysical characterization was performed for *Ci-βγ* and HγS in the presence of a variety of divalent cations to further investigate how the observed composition differences impact protein stability. Thermal unfolding curves were measured for both proteins via the 360 nm/320 nm ratio of tryptophan fluorescence intensities. Tryptophan side chains in nonpolar environments have a peak fluorescence near 320 nm, while those in highly polar environments, e.g., aqueous solution, fluoresce at 360 nm. All tryptophans in the folded structures of *Ci-βγ* and HγS are buried in the hydrophobic core of the protein; therefore, the ratio of fluorescence intensity at 360 nm to 320 nm as a function of temperature is a sensitive marker of protein unfolding, as previously demonstrated for *βγ*-crystallins.[88,89]

As previously reported, the $Ca^{2+}$-bound form of *Ci-βγ* has a greatly increased thermal unfolding midpoint ($T_m$) versus that of the apo form, with a dramatic increase from 46 to 94 °C[14] (Figure 5A). A similar stabilization was observed in the presence of $Sr^{2+}$, yielding a $T_m$ of 91 °C. Of the tested divalent metal cations, the next greatest $T_m$ was observed for $Mn^{2+}$ (84 °C) followed by $Mg^{2+}$ (71 °C), $Co^{2+}$ (70 °C), $Ni^{2+}$ (61 °C), and $Zn^{2+}$ (53 °C) (Figure 5B). For the tested cations, a higher $T_m$ was observed to correlate with a sharper unfolding transition. The exception to this trend was $Zn^{2+}$, where the *Ci-βγ* unfolding temperature range is similar to that of the $Sr^{2+}$- and $Ca^{2+}$-bound forms. The presence of $Ca^{2+}$ did not alter the $T_m$ of HγS (Figures 1D and 5C), consistent with its previously observed weak binding and the lack of changes to NMR chemical shifts upon addition of a cation.[14] None of the tested divalent cations alter the thermal unfolding behavior of HγS. The $T_m$ was ∼72 °C for all samples, consistent with previous literature reports.[90−92]

The wide range of effects on thermal stability of the divalent cations on *Ci-βγ* warrants some discussion of metal ion properties, given that all of these ions have a charge of +2 and are similar in size. Notably, the thermal stabilization from $Mn^{2+}$ is 12−13 °C greater than that due to $Mg^{2+}$. Examination of different metal ion properties indicates that stabilization of *Ci-βγ* correlates most strongly with coordination number, followed by ionic radius (Table 2). In other proteins, the native binding sites of $Mn^{2+}$ and $Mg^{2+}$ are most often BCH and BCB motifs, where binding is predominately coordinated via acid residues.[93] The lower-affinity binding of $Mn^{2+}$ and $Mg^{2+}$ to $Ca^{2+}$ coordination sites has been suggested to stem primarily from differences in ionic radius.[72] A small radius may alter the cation's interaction with some bidentate ligands. A similar argument can be made for $Sr^{2+}$ over $Mn^{2+}$, despite limited experimental data on $Sr^{2+}$ binding in proteins. Although its ionic radius is slightly larger than that of $Ca^{2+}$, $Sr^{2+}$ binding results in the same structural changes, with small reductions in ligand−cation coordination. Any minor changes in backbone coordination may then be accommodated by the flexibility of the aspartate and glutamate residues in the binding site.

**Divalent Cations Alter Thermal Aggregation in *Ci-βγ* and HγS.** Thermal gradient DLS was used to probe divalent cation-mediated changes in protein−protein interactions leading to the formation of soluble oligomers and insoluble aggregates. In DLS, a translational diffusion coefficient is measured via scattering correlation times, providing a sensitive tool for the detection of oligomer formation. γ-Crystallin aggregation under thermal stress often proceeds via a step function in which a sudden onset of oligomerization occurs



DOI: 10.1021/acs.biochem.9b00507
*Biochemistry* 2019, 58, 4505−4518

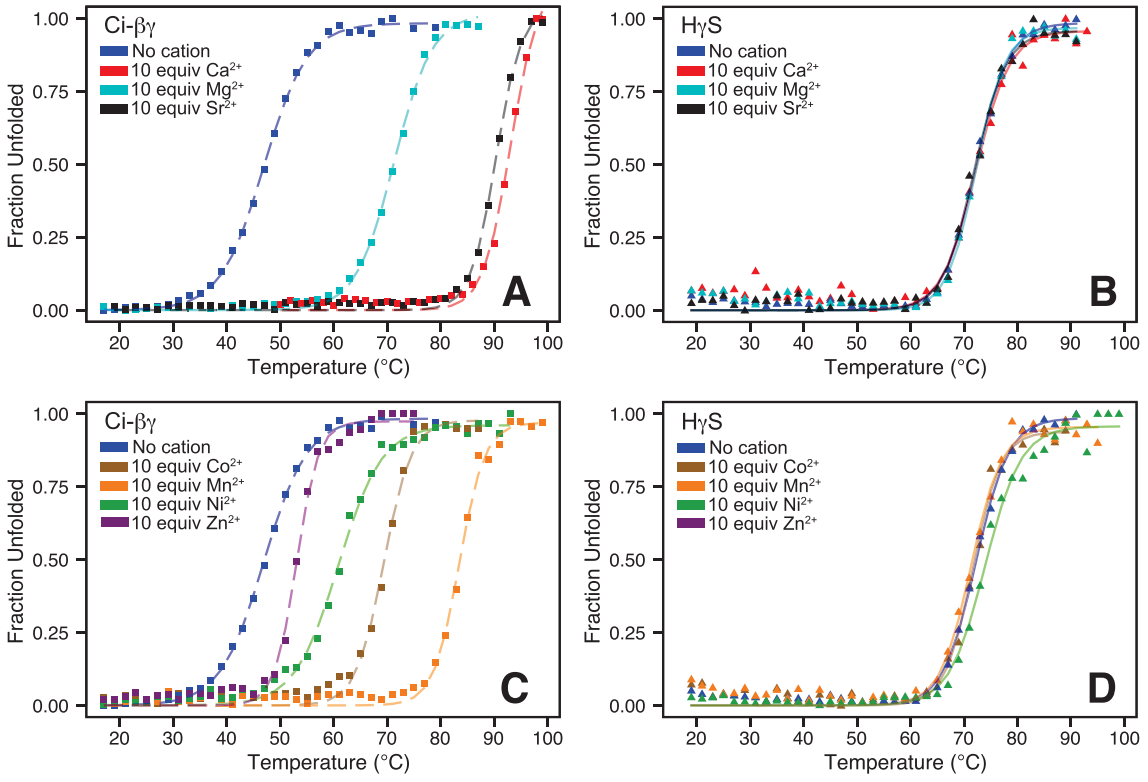


**Figure 5.** Protein thermal unfolding in the presence of 10 equiv of divalent cation. (A) *Ci-βγ* in the presence of $Ca^{2+}$ (red), $Mg^{2+}$ (aqua), $Sr^{2+}$ (black), or no cation (blue). (B) HγS in the presence of $Ca^{2+}$ (red), $Mg^{2+}$ (aqua), $Sr^{2+}$ (black), or no cation (blue). (C) *Ci-βγ* in the presence of $Co^{2+}$ (brown), $Mn^{2+}$ (orange), $Ni^{2+}$ (green), $Zn^{2+}$ (purple), or no cation (blue). (D) HγS in the presence of $Co^{2+}$ (brown), $Mn^{2+}$ (orange), $Ni^{2+}$ (green), or no cation (blue).

**Table 2. Divalent Cation Classification and Effect on *Ci-βγ* Unfolding**

| | $T_m$[a] (°C) | $T_i$[b] (°C) | ionic radius[c] (pm) | classification[d] | MESPUES CN[e] | CSD CN[f] |
|---|---|---|---|---|---|---|
| $Ca^{2+}$ | 94 | 82 | 100 | hard | 6–8 | 6, 7 |
| $Sr^{2+}$ | 91 | 79 | 118 | hard | – | 6, 8 |
| $Mn^{2+}$ | 84 | 72 | 83[g] | borderline | 6 | 6 |
| $Mg^{2+}$ | 71 | 58 | 72 | hard | 6 | 6 |
| $Co^{2+}$ | 70 | 55 | 74.5[h] | borderline | 6 | 4, 6 |
| $Ni^{2+}$ | 61 | 50 | 69 | borderline | 4 | 4, 6 |
| $Zn^{2+}$ | 53 | 40 | 74 | borderline | 4[i] | 4 |
| apo | 46 | 60 | – | – | – | |

[a]Thermal denaturation midpoint ($T_m$) determined via intrinsic fluorescence. [b]Initial temperature of aggregation ($T_i$) determined via DLS. [c]All ionic radius values are taken from ref 94 using the six-coordinate, 2+ charge state. [d]From Pearson's classification of hard and soft acids and bases.[95] [e]Coordination number (CN) collected from MESPEUS 10 and ref 96. [f]Coordination number (CN) taken from Tables 1–3 of ref 97 for frequencies of ≥33%. [g]High-spin ionic radius. [h]High-spin ionic radius. [i]Taken form Table 5 of ref 98.

directly from the monomeric population. We use the notation $T_i$ to refer to the initial temperature at which oligomers or aggregates form from the starting solution of monomers. These early stage soluble oligomers formed are 1–2 orders of magnitude larger in size than the monomers or dimers from which they were derived. These particles grow in size until they precipitate from solution, resulting in a decrease in scattering intensity, at which point the measurement was terminated.

Thermal unfolding data for *Ci-βγ*, in the apo form and bound to a variety of divalent cations, are shown in Figure 6A–C. The $T_i$ of apo-*Ci-βγ* occurs near 60 °C, resulting in 20 nm diameter oligomers. The oligomers remain soluble and increase in diameter to 50 nm at 92 °C. $Ca^{2+}$- and $Sr^{2+}$-bound *Ci-βγ* exhibit $T_i$ values of 82 and 79 °C, respectively, above which the oligomer diameter immediately exceeds 100 nm. The addition of $Mg^{2+}$ to *Ci-βγ* does not alter the $T_i$ (58 °C) relative to that of the apo form but yields 35 nm diameter oligomers. The soluble oligomers increase in size with an increase in temperature, with 50 nm oligomers forming at 70 °C. Of the tested transition metal cations, only $Mn^{2+}$ significantly increased the $T_i$ of *Ci-βγ*. As observed for $Ca^{2+}$ and $Sr^{2+}$, oligomers formed at the $T_i$ (70 °C) rapidly exceed the observable size. The addition of $Co^{2+}$, $Ni^{2+}$, or $Zn^{2+}$ reduces the $T_i$ of *Ci-βγ*. $Co^{2+}$ reduces the $T_i$ from 60 to 55 °C. The oligomers initially formed in the presence of $Co^{2+}$ are 30 nm in diameter and grow to 70 nm by 65 °C, above which the scattering signal is saturated. The $T_i$ values for $Ni^{2+}$ and $Zn^{2+}$ are 50 and 40 °C, respectively, where both form relatively small oligomers between 10 and 20 nm, with slow growth producing 50 nm oligomers at 70 °C. More rapid increases are observed at higher temperatures.

The analogous data for HγS are presented in Figure 6D–F. In the absence of divalent cations, HγS rapidly forms insoluble aggregates around 53 °C, consistent with prior studies of HγS alone.[91] The $T_i$ of HγS does not change in the presence of $Ca^{2+}$, $Sr^{2+}$, or $Mg^{2+}$; immediate formation of aggregates is observed in the presence of each of these cations. The transition metal divalent cations $Co^{2+}$ and $Ni^{2+}$ reduced the $T_i$ of HγS to 50 and 46 °C, respectively, whereas $Mn^{2+}$ did not



DOI: 10.1021/acs.biochem.9b00507
*Biochemistry* 2019, 58, 4505–4518

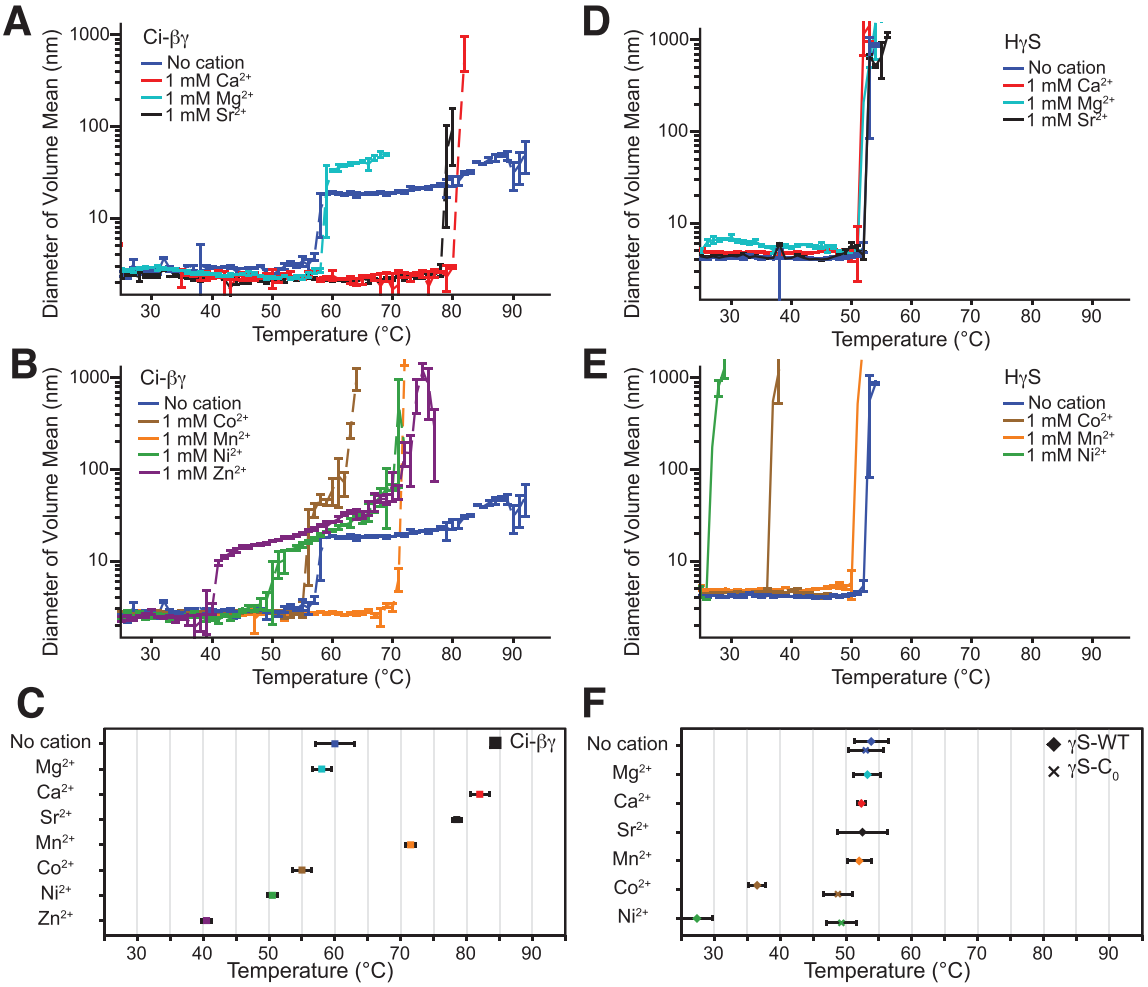


**Figure 6.** DLS was used to monitor the diameter of protein monomers and oligomers to access the temperature of aggregate formation under thermal stress and in the presence of 10 equiv of a divalent cation. (A) DLS measurements for *Ci-βγ* in the presence of $Ca^{2+}$ (red), $Mg^{2+}$ (aqua), $Sr^{2+}$ (black), or no cation (blue). (B) DLS of *Ci-βγ* in the presence of $Co^{2+}$ (brown), $Mn^{2+}$ (orange), $Ni^{2+}$ (green), $Zn^{2+}$ (purple), or no cation (blue). Each measurement trace reflects one representative measurement, where error bars correspond to one standard deviation collected from triplicate samples at each temperature. (C) Initial temperature of oligomer formation ($T_i$) for *Ci-βγ* under thermal stress measured via DLS. $T_i$ refers to the lowest temperature at which species larger than the native monomers are observed. This plot is derived from the data shown in panels A and B; this alternative visualization facilitates comparison of the aggregation onset temperatures and allows more straightforward presentation of the measurement error. Error bars represent one standard deviation. (D) DLS for HγS in the presence of $Ca^{2+}$ (red), $Mg^{2+}$ (aqua), $Sr^{2+}$ (black), or no cation (blue). (E) DLS of HγS in the presence of $Co^{2+}$ (brown), $Mn^{2+}$ (orange), $Ni^{2+}$ (green), or no cation (blue). (F) Initial temperature of oligomer formation ($T_i$) for HγS (diamonds) and HγS-$C_0$ (times signs), presented as in panel C.

alter the $T_i$. For all HγS measurements, the aggregate size rapidly exceeded 100 nm. The addition of $Zn^{2+}$ immediately produced large aggregates that precipitated out of solution; therefore, no DLS data are reported for treatment of HγS with this cation. Although *Ci-βγ*-crystallin resists $Cu^{2+}$-induced aggregation more effectively than γS-WT, >6 equiv results in light scattering (Figure S7). In comparison, $Zn^{2+}$ similarly aggregates γS-WT, whereas the presence of ≤10-fold $Zn^{2+}$ does not reduce the solubility of *Ci-βγ*. For the variant HγS-$C_0$, which does not contain solvent-accessible cysteines, the $T_i$ values in the presence of $Co^{2+}$ and $Ni^{2+}$ are both around 49 °C.

**$Zn^{2+}$-Driven Aggregation of HγS Proceeds through Cysteine Coordination, Whereas $Cu^{2+}$-Driven Aggregation Results from Methionine Oxidation.** In the healthy eye lens, γ-crystallins undergo only weak and transient interactions. Previous studies measuring interaction of γ-crystallin with exogenous peptides,[99] small molecules,[100] and cations[21] have highlighted the ability of the lens γ-crystallins to tolerate potentially destabilizing interactions to a certain extent; however, this capacity is limited, and aggregation results from excessive intermolecular contacts. We therefore focused on changes to protein solubility as a practical approach to determine the potential effects of divalent cations on γ-crystallin behavior. The addition of excess $Ca^{2+}$, $Sr^{2+}$, $Mg^{2+}$, and $Mn^{2+}$ did not alter the fluorescence or thermal unfolding of HγS, consistent with previous research demonstrating that HγD-crystallin does not aggregate upon addition of $Mn^{2+}$, $Fe^{2+}$, or $Ca^{2+}$,[21,101] and that γB- and γS-crystallins do not interact with $Ca^{2+}$.[14,60] $Co^{2+}$ and $Ni^{2+}$ did not alter the thermal unfolding of HγS but, when present in excess (6.5-fold), produced soluble aggregates under thermal stress and detectable light scattering after 2 h at 42 °C (Figure S8). The addition of $Zn^{2+}$ results in appreciable aggregation without thermal stress in low excess; therefore, further light scattering measurements were performed on the Cys to Ser variants HγS-$C_2$, HγS-$C_1$, and HγS-$C_0$, which were designed to test the



DOI: 10.1021/acs.biochem.9b00507
*Biochemistry* 2019, 58, 4505−4518

hypothesis that solvent-exposed cysteines are responsible for aggregation-promoting interactions with metal cations in HγS.

At room temperature, aggregates of HγS readily form following the addition of 5 equiv of $Zn^{2+}$ or 1 equiv of $Cu^{2+}$. Characterization of metal-induced aggregation was therefore measured via light scattering at 405 nm. Zinc-induced aggregation of HγS was measured for the monomeric and dimeric forms (Figure 7). One equivalent of $Zn^{2+}$ produced

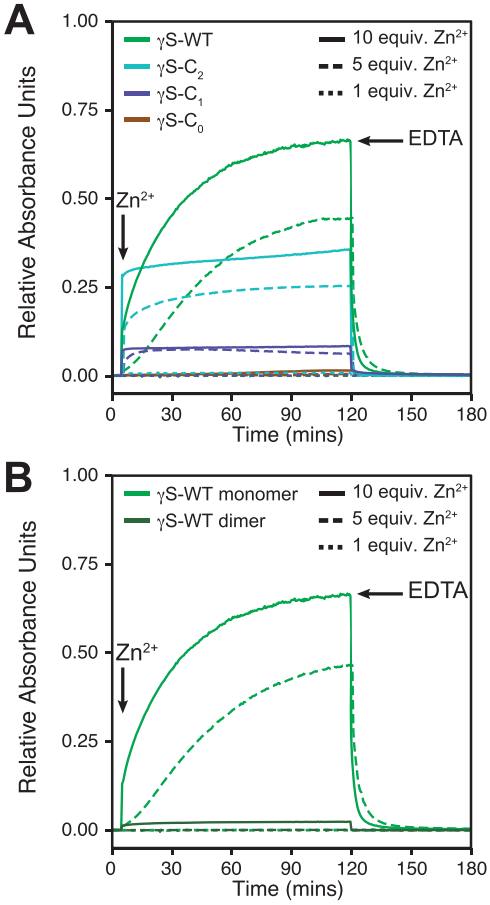


**Figure 7.** Treatment of human γS-crystallin and its cysteine-to-serine variants with 1 equiv (small dash lines), 5 equiv (long dash lines), or 10 equiv (solid lines) of $Zn^{2+}$. (A) Light scattering of monomeric HγS wild type (green), HγS-$C_2$ (cyan), HγS-$C_1$ (purple), and HγS-$C_0$ (brown). (B) Light scattering of monomeric HγS (green) and dimeric HγS (dark green). The HγS wild-type dimer was collected from the protein purification process without further modification.

limited aggregation of monomeric HγS, while 5 and 10 equiv induced elevated levels of light scattering. Upon addition of 10 equiv, but not 5 equiv, of $Zn^{2+}$, a small increase in light scattering of HγS dimers was observed. Similar measurements were performed using monomeric HγS-$C_2$, HγS-$C_1$, and HγS-$C_0$. Similar to HγS-WT, each of the Cys-to-Ser variants produced negligible aggregation in the presence of 1 equiv of $Zn^{2+}$. Appreciable γS-$C_2$ aggregation was observed for the addition of 10 equiv of $Zn^{2+}$, while 5 equiv produced slightly less aggregation. Ten and 5 equiv of $Zn^{2+}$ yielded similarly low levels of aggregation for γS-$C_1$, while detectable aggregation of γS-$C_0$ could be observed at 2 h with 10 equiv. For all proteins and zinc ion equivalents, the addition of EDTA reduced the light scattering intensity to background levels (Figure 7).

The removal of surface-exposed cysteines in HγS-$C_0$ abrogated $Zn^{2+}$-mediated aggregation (Figure 7A) as well as $Ni^{2+}$- and $Co^{2+}$-induced aggregation under mild thermal stress. For all proteins tested, $Zn^{2+}$ aggregation was reversible upon addition of EDTA (Figure 7B), supporting our hypothesis that zinc ions coordinate to HγS via solvent-accessible cysteines and cause intermolecular bridging. Dimerization of HγS, presumably via C25 disulfide bond formation, limits cysteine solvent accessibility. The dramatically reduced level of aggregation in HγS dimer-only solutions further supports the idea that cysteine solvent accessibility regulates $Zn^{2+}$-mediated intermolecular bridging aggregation. Dominguez et al. previously reported that $Zn^{2+}$ induces trace aggregation of HγS but did not specify the extent of dimerization.[101] Therefore, we suspect that dimerization is responsible for the discrepancy between our results and those reported in this prior study.

Although Hγ-WT aggregates to a greater total extent than HγS-$C_2$ or HγS−$C_1$, it does so more slowly. We hypothesize that $Zn^{2+}$ may interact with the more buried C23 (21% SASA) or C27 (40% SASA), resulting in a smaller solvent-accessible surface area for the zinc ion. In this case, the clustered cysteines may serve as a weak buffer against intermolecular bridging. In HγS-$C_2$ and HγS-$C_1$, where the remaining solvent-exposed cysteines are not spatially proximal to each other, most of the increase in light scattering occurs immediately. For these two variants, the extent of aggregation is considerably reduced despite a higher ratio of $Zn^{2+}$ to solvent-accessible cysteines.

In addition to $Zn^{2+}$, we also observed $Cu^{2+}$-induced aggregation of HγS. The addition of 1 equiv of $Cu^{2+}$ produced considerable levels of aggregation for HγS-WT and each Cys-to-Ser variant (Figure S9), to the extent that precipitation occurred. The dimer of HγS-WT exhibited similar total aggregation under the same conditions. Prior investigations of γD-crystallin have shown that the solvent-accessible residues C109 and C111 are primarily responsible for $Cu^{2+}$-induced aggregation, which can be blocked using GSSG.[22] The disappearance of $^{1}H-^{15}N$ HSQC peak intensity in HγD prepared with $Cu^{2+}$ provides further evidence that the strongest interactions occur at the solvent-accessible cysteines.[21] We felt confident that the removal of the solvent-accessible cysteines in γS-crystallin, which we observed led to decreased levels of $Zn^{2+}$-induced aggregation, would have a similar effect for $Cu^{2+}$. However, this hypothesis proved to be incorrect. In contrast to $Zn^{2+}$, the removal or reduction of solvent-accessible cysteine side chains does not strongly impact $Cu^{2+}$-induced aggregation, although the scattering intensity of all samples is decreased upon addition of EDTA, suggesting that superficial cross-linking is partially responsible. No changes in protein structure are evident upon the addition of either $Cu^{2+}$ or $Zn^{2+}$ for HγS-WT based on far-UV circular dichroism (Figure S10).

To further investigate the mechanism of $Cu^{2+}$-induced aggregation, we digested the insoluble aggregates of HγS-WT and HγS-$C_0$ with trypsin to search for oxidative PTMs or modifications observed in aged lenses via mass spectrometry (Table S8 and Figure S11). The light-scattering samples of HγS and HγS-$C_0$ incubated with 10 equiv of $Cu^{2+}$ were analyzed via mass spectrometry to determine if PTMs were present. Trypsin digests were performed using the HγS-WT and HγS-$C_0$ pellets collected via centrifugation with MS/MS mapping to confirm PTMs. Mass shifts of +16 and +32 Da



DOI: 10.1021/acs.biochem.9b00507
Biochemistry 2019, 58, 4505−4518

(corresponding to cysteine oxidation) for peptides containing C23, C25, C27, and C115 were the only modifications investigated from the HγS-WT digest. Across several measurements, MS/MS mapping of modification showed C25 was the most consistently modified of the C23−C25−C27 triad. Digests of γS-$C_0$ produced fewer detectable mass-shifted peptides. The observed shifts of +16 Da were observed for two peptides, corresponding to oxidation of M59 and M124. Why these two methionines are more readily oxidized than M74, M108, or M119 is yet unclear, given that the latter residues all have a larger solvent-accessible surface area. We speculate that local electrostatics are involved; however, further investigation is required.

Functional characterization of the interactions of *Ci-βγ* is highly relevant to understanding its role in the tunicate sensory vesicle. This structure, which contains both the ocellus and the otolith, is highly enriched in several metal cations, including $Ca^{2+}$ and $Zn^{2+}$ as a means of controlling its specific gravity.[4] We previously reported that the fluorescence intensity of *Ci-βγ* changes in response to $Ca^{2+}$ binding; therefore, a preliminary analysis of fluorescence intensity changes was performed using $Mg^{2+}$, $Sr^{2+}$, $Mn^{2+}$, $Co^{2+}$, $Ni^{2+}$, and $Zn^{2+}$ (Figure S12). The changes in *Ci-βγ* fluorescence intensity were comparable to those observed upon binding $Ca^{2+}$, prompting us to continue with thermal unfolding and aggregation measurements. Interestingly, thermal aggregates of apo-*Ci-βγ* do not form until 60 °C, despite its thermal unfolding midpoint of 46 °C. The addition of divalent cations reverses this trend, resulting in its $T_m$ being 10−15 °C lower than its $T_i$ (Figure 5 and Table 2). The persistence of this trend, independent of the degree of thermal stabilization, suggests that the underlying interactions of *Ci-βγ* with different divalent cations are highly similar. In addition, the difference in aggregate size between apo-*Ci-βγ* (<50 nm) and cation-bound *Ci-βγ* (>1000 nm) suggests that increased structural rigidity may alter the aggregation pathway.

## CONCLUSION

The double-clamp motif of the *βγ*-crystallin domain is capable of binding to a broad range of divalent cations beyond $Ca^{2+}$. This functionality is aided by the absence of readily oxidizable and cation-coordinating residues such as cysteine, histidine, and methionine. In contrast, vertebrate lens γ-crystallins, which mostly do not bind divalent metal cations, are structurally similar but compositionally different. Notably, the amino acid composition of the lens γ-crystallins favors more refractive residues, and their sequences were apparently not shaped by selective pressure against cysteines. In human γS-crystallin, solvent-exposed cysteine residues increase the susceptibility to $Zn^{2+}$-induced aggregation through cross-linking, whereas $Cu^{2+}$-induced aggregation is driven by methionine oxidation.

## ASSOCIATED CONTENT

### Supporting Information

The Supporting Information is available free of charge on the ACS Publications website at DOI: 10.1021/acs.biochem.9b00507.

Additional biophysical characterization and sequence analysis data (PDF)

### Accession Codes

Uniprot CRYGS_HUMAN, F6Q2R9_CION.

## AUTHOR INFORMATION


### Corresponding Author

*E-mail: rachel.martin@uci.edu.

### ORCID

Rachel W. Martin: 0000-0001-9996-7411



### Funding

This work was supported by National Science Foundation Grants DMR-1410415 to R.W.M. and D. J. Tobias and DMS-1361425 to R.W.M. and C. T. Butts and National Institutes of Health Grant 1R01EY025328 to R.W.M. and D. J. Tobias. K.R. was supported by National Science Foundation Grant DGE-1633631. R.W.M. is a CIFAR fellow.


### Notes

The authors declare no competing financial interest.

## ACKNOWLEDGMENTS


The authors thank Dmitry Fishman for excellent management of the UCI Laser Spectroscopy Laboratories, Felix Grun and Ben Katz for excellent management of the Mass Spectrometry Facility, and Stephen White and Celia Goulding for access to the ITC instruments.


## ADDITIONAL NOTE

[a]Amino acid indices referenced in this paper include the glycine at the first position that is left after TEV cleavage. This glycine is in the position where a start methionine would be and is often not included in the sequence numbering. The numbering used here therefore differs from those of some other γS-crystallin references by 1.

## REFERENCES


(1) Wistow, G., Summers, L., and Blundell, T. (1985) *Myxococcus xanthus* spore coat protein S may have a similar structure to vertebrate lens *βγ*-crystallins. *Nature 315*, 771−773.

(2) Wistow, G. (1990) Evolution of a protein superfamily: relationships between vertebrate lens crystallins and microorganism dormancy proteins. *J. Mol. Evol. 30*, 140−145.

(3) Esposito, R., Racioppi, C., Pezzotti, M., Branno, M., Locascio, A., Ristoratore, F., and Spagnuolo, A. (2015) The ascidian pigmented sensory organs: Structures and developmental programs. *Genesis 53*, 15−33.

(4) Sakurai, D., Goda, M., Kohmura, Y., Horie, T., Iwamoto, H., Ohtsuki, H., and Tsuda, M. (2004) The role of pigment cells in the brain of ascidian larva. *J. Comp. Neurol. 475*, 70−82.

(5) Coniglio, L., Morale, A., Angelini, C., and Falugi, C. (1998) Cholinergic activation of settlement in *Ciona intestinalis* metamorphosing larvae. *J. Exp. Zool. 280*, 314−320.

(6) Shimeld, S. M., Purkiss, A. G., Dirks, R. P., Bateman, O. A., Slingsby, C., and Lubsen, N. H. (2005) Urochordate *βγ*-Crystallin and the evolutionary origin of the vertebrate eye lens. *Curr. Biol. 15*, 1684−1689.

(7) Khago, D., Bierma, J. C., Roskamp, K. W., Kozlyuk, N., and Martin, R. W. (2018) Protein refractive index increment is determined by conformation as well as composition. *J. Phys.: Condens. Matter 30*, 435101.

(8) Mishra, A., Krishnan, B., Raman, R., and Sharma, Y. (2016) $Ca^{2+}$ and *βγ*-crystallins: An affair that did not last? *Biochim. Biophys. Acta, Gen. Subj. 1860*, 299−303.

(9) Slingsby, C., Wistow, G. J., and Clark, A. R. (2013) Evolution of crystallins for a role in the vertebrate eye lens. *Protein Sci. 22*, 367−380.

(10) Barnwal, R. P., Jobby, M. K., Sharma, Y., and Chary, K. V. (2006) NMR Assignment of M-Crystallin: A Novel $Ca^{2+}$ Binding Protein of the *βγ*-Crystallin Superfamily from *Methanosarcina acetivorans*. *J. Biomol. NMR 36*, 32−32.




DOI: 10.1021/acs.biochem.9b00507
*Biochemistry* 2019, 58, 4505−4518

(11) Suman, S. K., Ravindra, D., Sharma, Y., and Mishra, A. (2013) Association properties and unfolding of a βγ-Crystallin domain of a Vibrio-specific protein. *PLoS One 8*, e53610.
(12) Jobby, M. K., and Sharma, Y. (2007) Calcium-binding to lens βB2-and βA3-crystallins suggests that all β-crystallins are calcium-binding proteins. *FEBS J. 274*, 4135−4147.
(13) Rajini, B., Shridas, P., Sundari, C. S., Muralidhar, D., Chandani, S., Thomas, F., and Sharma, Y. (2001) Calcium binding properties of γ-Crystallin: calcium ion binds at the Greek key βγ-Crystallin fold. *J. Biol. Chem. 276*, 38464−38471.
(14) Kozlyuk, N., Sengupta, S., Bierma, J. C., and Martin, R. W. (2016) Calcium binding dramatically stabilizes an ancestral Crystallin fold in tunicate βγ-Crystallin. *Biochemistry 55*, 6961−6968.
(15) Piatigorsky, J. (1984) Delta crystallins and their nucleic acids. *Mol. Cell. Biochem. 59*, 33−56.
(16) Chiou, S.-H., Chang, W., and Chen, C. (1989) Characterization and comparison of epsilon-Crystallin and lactate dehydrogenases in the lenses of vertebrates and invertebrates. *Biochem. Int. 18*, 1093−1100.
(17) Huang, Q.-L., Russell, P., Stone, S., and Zigler, J. (1987) Zeta-Crystallin, a novel lens protein from the guinea pig. *Curr. Eye Res. 6*, 725−732.
(18) Mulders, J., Hendriks, W., Blankesteijn, W. M., Bloemendal, H., and de Jong, W. W. (1988) Lambda-Crystallin, a major rabbit lens protein, is related to hydroxyacyl-coenzyme A dehydrogenases. *J. Biol. Chem. 263*, 15462−15466.
(19) Wistow, G. J., Lietman, T., Williams, L. A., Stapel, S. O., De Jong, W. W., Horwitz, J., and Piatigorsky, J. (1988) Tau-Crystallin/alpha-enolase: one gene encodes both an enzyme and a lens structural protein. *J. Cell Biol. 107*, 2729−2736.
(20) Ghosh, K. S., Pande, A., and Pande, J. (2011) Binding of γ-Crystallin substrate prevents the binding of copper and zinc ions to the molecular chaperone α-Crystallin. *Biochemistry 50*, 3279−3281.
(21) Quintanar, L., Dominguez-Calva, J. A., Serebryany, E., Rivillas-Acevedo, L., Haase-Pettingell, C., Amero, C., and King, J. A. (2016) Copper and zinc ions specifically promote nonamyloid aggregation of the highly stable human γD-Crystallin. *ACS Chem. Biol. 11*, 263−272.
(22) Ramkumar, S., Fan, X., Wang, B., Yang, S., and Monnier, V. M. (2018) Reactive cysteine residues in the oxidative dimerization and $Cu^{2+}$ induced aggregation of human γD-Crystallin: Implications for age-related cataract. *Biochim. Biophys. Acta, Mol. Basis Dis. 1864*, 3595−3604.
(23) Lin, J. (1997) Pathophysiology of cataracts: copper ion and peroxidation in diabetics. *Jpn. J. Ophthalmol. 41*, 130−137.
(24) Aydin, E., Cumurcu, T., Özuĝurlu, F., Özyurt, H., Sahinoglu, S., Mendil, D., and Hasdemir, E. (2005) Levels of iron, zinc, and copper in aqueous humor, lens, and serum in nondiabetic and diabetic patients. *Biol. Trace Elem. Res. 108*, 033−041.
(25) Cekic, O. (1998) Effect of cigarette smoking on copper, lead, and cadmium accumulation in human lens. *Br. J. Ophthalmol. 82*, 186−188.
(26) Dawczynski, J., Blum, M., Winnefeld, K., and Strobel, J. (2002) Increased content of zinc and iron in human cataractous lenses. *Biol. Trace Elem. Res. 90*, 15−23.
(27) Schmeling, M., Gaynes, B. I., and Tidow-Kebritchi, S. (2014) Heavy metal analysis in lens and aqueous humor of cataract patients by total reflection X-ray fluorescence spectrometry. *Powder Diffr. 29*, 155−158.
(28) Domínguez-Calva, J., Pérez-Vázquez, M., Serebryany, E., King, J., and Quintanar, L. (2018) Mercury-induced aggregation of human lens γ-crystallins reveals a potential role in cataract disease. *JBIC, J. Biol. Inorg. Chem. 23*, 1105−1118.
(29) Brazier, M. W., Davies, P., Player, E., Marken, F., Viles, J. H., and Brown, D. R. (2008) Manganese binding to the prion protein. *J. Biol. Chem. 283*, 12831−12839.
(30) Barnwal, R. P., Jobby, M., Devi, K. M., Sharma, Y., and Chary, K. V. (2009) Solution structure and calcium-binding properties of M-Crystallin, a primordial βγ-Crystallin from archaea. *J. Mol. Biol. 386*, 675−689.
(31) Aravind, P., Mishra, A., Suman, S. K., Jobby, M. K., Sankaranarayanan, R., and Sharma, Y. (2009) The βγ-Crystallin superfamily contains a universal motif for binding calcium. *Biochemistry 48*, 12180−12190.
(32) Kretschmar, M., Mayr, E.-M., and Jaenicke, R. (1999) Kinetic and thermodynamic stabilization of the βγ-Crystallin homolog spherulin 3a from *Physarum polycephalum* by calcium binding. *J. Mol. Biol. 289*, 701−705.
(33) Wenk, M., Baumgartner, R., Holak, T. A., Huber, R., Jaenicke, R., and Mayr, E.-M. (1999) The domains of protein S from *Myxococcus xanthus*: structure, stability and interactions. *J. Mol. Biol. 286*, 1533−1545.
(34) Riyahi, K., and Shimeld, S. M. (2007) Chordate βγ-crystallins and the evolutionary developmental biology of the vertebrate lens. *Comp. Biochem. Physiol., Part B: Biochem. Mol. Biol. 147*, 347−357.
(35) Snyder, E. E., Buoscio, B. W., and Falke, J. J. (1990) Calcium (II) site specificity: effect of size and charge on metal ion binding to an EF-hand-like site. *Biochemistry 29*, 3937−3943.
(36) Park, C.-S., and MacKinnon, R. (1995) Divalent cation selectivity in a cyclic nucleotide-gated ion channel. *Biochemistry 34*, 13328−13333.
(37) Brunet, S., Scheuer, T., Klevit, R., and Catterall, W. A. (2005) Modulation of CaV1. 2 channels by $Mg^{2+}$ acting at an EF-hand motif in the COOH-terminal domain. *J. Gen. Physiol. 126*, 311−323.
(38) Dove, S., and Kingsford, M. (1998) Use of otoliths and eye lenses for measuring trace-metal incorporation in fishes: a biogeographic study. *Mar. Biol. 130*, 377−387.
(39) Clout, N. J., Kretschmar, M., Jaenicke, R., and Slingsby, C. (2001) Crystal structure of the calcium-loaded spherulin 3a dimer sheds light on the evolution of the eye lens βγ-Crystallin domain fold. *Structure 9*, 115−124.
(40) Vergara, A., Grassi, M., Sica, F., Pizzo, E., D'Alessio, G., Mazzarella, L., and Merlino, A. (2013) A novel interdomain interface in crystallins: structural characterization of the βγ-Crystallin from *Geodia cydonium* at 0.99 Å resolution. *Acta Crystallogr., Sect. D: Biol. Crystallogr. 69*, 960−967.
(41) Kumar, S., Stecher, G., and Tamura, K. (2016) MEGA7: molecular evolutionary genetics analysis version 7.0 for bigger datasets. *Mol. Biol. Evol. 33*, 1870−1874.
(42) Edgar, R. C. (2004) MUSCLE: multiple sequence alignment with high accuracy and high throughput. *Nucleic acids research 32*, 1792−1797.
(43) Pond, S. L. K., and Muse, S. V. (2005) *Statistical Methods in Molecular Evolution*, pp 125−181, Springer.
(44) Willard, L., Ranjan, A., Zhang, H., Monzavi, H., Boyko, R. F., Sykes, B. D., and Wishart, D. S. (2003) VADAR: a web server for quantitative evaluation of protein structure quality. *Nucleic Acids Res. 31*, 3316−3319.
(45) Ebersbach, H., Fiedler, E., Scheuermann, T., Fiedler, M., Stubbs, M. T., Reimann, C., Proetzel, G., Rudolph, R., and Fiedler, U. (2007) Affilin−novel binding molecules based on human γ-B-Crystallin, an all β-sheet protein. *J. Mol. Biol. 372*, 172−185.
(46) Dixit, K., Pande, A., Pande, J., and Sarma, S. P. (2016) Nuclear Magnetic Resonance Structure of a Major Lens Protein, Human γC-Crystallin: Role of the Dipole Moment in Protein Solubility. *Biochemistry 55*, 3136−3149.
(47) Basak, A., Bateman, O., Slingsby, C., Pande, A., Asherie, N., Ogun, O., Benedek, G. B., and Pande, J. (2003) High-resolution X-ray crystal structures of human γD Crystallin (1.25 Å) and the R58H mutant (1.15 Å) associated with aculeiform cataract. *J. Mol. Biol. 328*, 1137−1147.
(48) Brubaker, W. D., and Martin, R. W. (2012) $^{1}H$, $^{13}C$, and $^{15}N$ assignments of wild-type human γS-Crystallin and its cataract-related variant γS-G18V. *Biomol. NMR Assignments 6*, 63−67.
(49) Zhang, Y. (2008) I-TASSER server for protein 3D structure prediction. *BMC Bioinf. 9*, 40.
(50) Studier, F. W. (2005) Protein production by auto-induction in high-density shaking cultures. *Protein Expression Purif. 41*, 207−234.


DOI: 10.1021/acs.biochem.9b00507
*Biochemistry* 2019, 58, 4505−4518

(51) Thorn, D. C., Grosas, A. B., Mabbitt, P. D., Ray, N. J., Jackson, C. J., and Carver, J. A. (2019) The structure and stability of the disulfide-linked γS-Crystallin dimer provide insight into oxidation products associated with lens cataract formation. *J. Mol. Biol. 431*, 483−497.
(52) Hains, P. G., and Truscott, R. J. (2007) Post-translational modifications in the nuclear region of young, aged, and cataract human lenses. *J. Proteome Res. 6*, 3935−3943.
(53) Wilmarth, P., Tanner, S., Dasari, S., Nagalla, S., Riviere, M., Bafna, V., Pevzner, P., and David, L. (2006) Age-related changes in human crystallins determined from comparative analysis of post-translational modifications in young and aged lens: does deamidation contribute to Crystallin insolubility? *J. Proteome Res. 5*, 2554−2566.
(54) Madian, A. G., and Regnier, F. E. (2010) Proteomic identification of carbonylated proteins and their oxidation sites. *J. Proteome Res. 9*, 3766−3780.
(55) Pitt, A. R., and Spickett, C. M. (2008) Mass spectrometric analysis of HOCl-and free-radical-induced damage to lipids and proteins. *Biochem. Soc. Trans. 36*, 1077−1082.
(56) Sun, H., Ma, Z., Li, Y., Liu, B., Li, Z., Ding, X., Gao, Y., Ma, W., Tang, X., Li, X., and Shen, Y. (2005) Gamma-S Crystallin gene (CRYGS) mutation causes dominant progressive cortical cataract in humans. *Journal of Medical Genetics 42*, 706−710.
(57) Devi, R. R., Yao, W., Vijayalakshmi, P., Sergeev, Y. V., Sundaresan, P., and Hejtmancik, J. F. (2008) Crystallin gene mutations in Indian families with inherited pediatric cataract. *Mol. Vision 14*, 1157−1170.
(58) Vendra, V. P. R., Khan, I., Chandani, S., Muniyandi, A., and Balasubramanian, D. (2016) Gamma crystallins of the human eye lens. *Biochim. Biophys. Acta, Gen. Subj. 1860*, 333−343.
(59) Ji, F., Jung, J., and Gronenborn, A. M. (2012) Structural and biochemical characterization of the childhood cataract-associated R76S mutant of human γD-Crystallin. *Biochemistry 51*, 2588−2596.
(60) Suman, S. K., Mishra, A., Ravindra, D., Yeramala, L., and Sharma, Y. (2011) Evolutionary remodelling of the betagamma-crystallins for domain stability at the cost of $Ca^{2+}$-binding. *J. Biol. Chem. 286*, 43891−43901.
(61) Suman, S. K., Mishra, A., Yeramala, L., Rastogi, I. D., and Sharma, Y. (2013) Disability for function: loss of $Ca^{2+}$-binding is obligatory for fitness of mammalian βγ-crystallins. *Biochemistry 52*, 9047−9058.
(62) Srivastava, S. S., Mishra, A., Krishnan, B., and Sharma, Y. (2014) $Ca^{2+}$-binding Motif of βγ-Crystallins. *J. Biol. Chem. 289*, 10958−10966.
(63) Kozlov, K. (2001) Vertebrate Crystallins−from Proteins to Genes. *Russ. J. Dev. Biol. 32*, 265−282.
(64) Wistow, G. (2012) The human Crystallin gene families. *Hum. Genomics 6*, 26.
(65) Shu, N., Zhou, T., and Hovmöller, S. (2008) Prediction of zinc-binding sites in proteins from sequence. *Bioinformatics 24*, 775−782.
(66) Keenan, J., Orr, D., and Pierscionek, B. (2008) Patterns of Crystallin distribution in porcine eye lenses. *Mol. Vision 14*, 1245−1253.
(67) Chen, Y., Zhao, H., Schuck, P., and Wistow, G. (2014) Solution properties of γ-crystallins: Compact structure and low frictional ratio are conserved properties of diverse γ-crystallins. *Protein Sci. 23*, 76−87.
(68) Zhao, H., Brown, P. H., and Schuck, P. (2011) On the distribution of protein refractive index increments. *Biophys. J. 100*, 2309−2317.
(69) Serebryany, E., Yu, S., Trauger, S. A., Budnik, B., and Shakhnovich, E. I. (2018) Dynamic disulfide exchange in a Crystallin protein in the human eye lens promotes cataract-associated aggregation. *J. Biol. Chem. 293*, 17997−18009.
(70) Lapko, V. N., Smith, D. L., and Smith, J. B. (2003) Methylation and carbamylation of human γ-crystallins. *Protein Sci. 12*, 1762−1774.
(71) Kosakovsky Pond, S. L., and Frost, S. D. (2005) Not so different after all: a comparison of methods for detecting amino acid sites under selection. *Mol. Biol. Evol. 22*, 1208−1222.
(72) Senguen, F. T., and Grabarek, Z. (2012) X-ray structures of magnesium and manganese complexes with the N-terminal domain of calmodulin: insights into the mechanism and specificity of metal ion binding to an EF-hand. *Biochemistry 51*, 6182−6194.
(73) Lewit-Bentley, A., and Réty, S. (2000) EF-hand calcium-binding proteins. *Curr. Opin. Struct. Biol. 10*, 637−643.
(74) Fukuda, M., Kojima, T., and Mikoshiba, K. (1997) Regulation by bivalent cations of phospholipid binding to the C2A domain of synaptotagmin III. *Biochem. J. 323*, 421−425.
(75) Teintze, M., Inouye, M., and Inouye, S. (1988) Characterization of calcium-binding sites in development-specific protein S of *Myxococcus xanthus* using site-specific mutagenesis. *J. Biol. Chem. 263*, 1199−1203.
(76) Jobby, M. K., and Sharma, Y. (2005) Calcium-binding crystallins from *Yersinia pestis*: characterization of two single βγ-Crystallin domains of a putative exported protein. *J. Biol. Chem. 280*, 1209−1216.
(77) Feng, M., Patel, D., Dervan, J., Ceska, T., Suck, D., Haq, I., and Sayers, J. (2004) Roles of divalent metal ions in flap endonuclease−substrate interactions. *Nat. Struct. Mol. Biol. 11*, 450−456.
(78) Chao, Y., and Fu, D. (2004) Thermodynamic studies of the mechanism of metal binding to the *Escherichia coli* zinc transporter YiiP. *J. Biol. Chem. 279*, 17173−17180.
(79) Basak, P., Debnath, T., Banerjee, R., and Bhattacharyya, M. (2016) Selective binding of divalent cations toward heme proteins. *Front. Biol. 11*, 32−42.
(80) Huang, X., and Miller, W. (1991) A time-efficient, linear-space local similarity algorithm. *Advances in Applied Mathematics 12*, 337−357.
(81) Bodenhausen, G., and Ruben, D. (1980) Natural abundance nitrogen-15 NMR by enhanced heteronuclear spectroscopy. *Chem. Phys. Lett. 69*, 185−189.
(82) Nara, M., Tanokura, M., Yamamoto, T., and Tasumi, M. (1995) A comparative study of the binding effects of $Mg^{2+}$, $Ca^{2+}$, $Sr^{2+}$, and $Cd^{2+}$ on calmodulin by fourier-transform infrared spectroscopy. *Biospectroscopy 1*, 47−54.
(83) Chao, S. H., Suzuki, Y., Zysk, J. R., and Cheung, W. (1984) Activation of calmodulin by various metal cations as a function of ionic radius. *Mol. Pharmacol. 26*, 75−82.
(84) Ozawa, T., Sasaki, K., and Umezawa, Y. (1999) Metal ion selectivity for formation of the calmodulin−metal−target peptide ternary complex studied by surface plasmon resonance spectroscopy. *Biochim. Biophys. Acta, Protein Struct. Mol. Enzymol. 1434*, 211−220.
(85) Yamniuk, A. P., Nguyen, L. T., Hoang, T. T., and Vogel, H. J. (2004) Metal ion binding properties and conformational states of calcium-and integrin-binding protein. *Biochemistry 43*, 2558−2568.
(86) Yamniuk, A. P., Silver, D. M., Anderson, K. L., Martin, S. R., and Vogel, H. J. (2007) Domain stability and metal-induced folding of calcium-and integrin-binding protein 1. *Biochemistry 46*, 7088−7098.
(87) Blancuzzi, Y., Padilla, A., Cave, A., and Parello, J. (1993) Symmetrical rearrangement of the cation-binding sites of parvalbumin upon calcium/magnesium exchange. A study by proton 2D NMR. *Biochemistry 32*, 1302−1309.
(88) Kosinski-Collins, M. S., Flaugh, S. L., and King, J. (2004) Probing folding and fluorescence quenching in human γD Crystallin Greek key domains using triple tryptophan mutant proteins. *Protein Sci. 13*, 2223−2235.
(89) Flaugh, S. L., Kosinski-Collins, M. S., and King, J. (2005) Contributions of hydrophobic domain interface interactions to the folding and stability of human γD-Crystallin. *Protein Sci. 14*, 569−581.
(90) Ma, Z., Piszczek, G., Wingfield, P. T., Sergeev, Y. V., and Hejtmancik, J. F. (2009) The G18V CRYGS mutation associated with human cataracts increases γS-Crystallin sensitivity to thermal and chemical stress. *Biochemistry 48*, 7334−7341.
(91) Brubaker, W. D., Freites, J. A., Golchert, K. J., Shapiro, R. A., Morikis, V., Tobias, D. J., and Martin, R. W. (2011) Separating instability from aggregation propensity in γS-Crystallin variants. *Biophys. J. 100*, 498−506.


DOI: 10.1021/acs.biochem.9b00507
*Biochemistry* 2019, 58, 4505−4518

(92) Ray, N. J., Hall, D., and Carver, J. A. (2016) Deamidation of N76 in human γS-Crystallin promotes dimer formation. *Biochim. Biophys. Acta, Gen. Subj. 1860*, 315−324.
(93) Khrustalev, V. V., Barkovsky, E. V., and Khrustaleva, T. A. (2016) Magnesium and manganese binding sites on proteins have the same predominant motif of secondary structure. *J. Theor. Biol. 395*, 174−185.
(94) Shannon, R. D. (1976) Revised effective ionic radii and systematic studies of interatomic distances in halides and chalcogenides. *Acta Crystallogr., Sect. A: Cryst. Phys., Diffr., Theor. Gen. Crystallogr. 32*, 751−767.
(95) Pearson, R. G. (1963) Hard and soft acids and bases. *J. Am. Chem. Soc. 85*, 3533−3539.
(96) Hsin, K., Sheng, Y., Harding, M., Taylor, P., and Walkinshaw, M. (2008) MESPEUS: a database of the geometry of metal sites in proteins. *J. Appl. Crystallogr. 41*, 963−968.
(97) Dudev, M., Wang, J., Dudev, T., and Lim, C. (2006) Factors governing the metal coordination number in metal complexes from Cambridge Structural Database analyses. *J. Phys. Chem. B 110*, 1889−1895.
(98) Harding, M. M. (2001) Geometry of metal−ligand interactions in proteins. *Acta Crystallogr., Sect. D: Biol. Crystallogr. 57*, 401−411.
(99) Banerjee, P. R., Pande, A., Shekhtman, A., and Pande, J. (2015) Molecular mechanism of the chaperone function of mini-α-Crystallin, a 19-residue peptide of human α-Crystallin. *Biochemistry 54*, 505−515.
(100) Khago, D., Wong, E. K., Kingsley, C. N., Alfredo Freites, J., Tobias, D. J., and Martin, R. W. (2016) Increased hydrophobic surface exposure in the cataract-related G18V variant of human γS-Crystallin. *Biochim. Biophys. Acta, Gen. Subj. 1860*, 325−332.
(101) Domínguez-Calva, J. A., Haase-Pettingell, C., Serebryany, E., King, J. A., and Quintanar, L. (2018) A histidine switch for Zn-induced aggregation of γ-crystallins reveals a metal-bridging mechanism relevant to cataract disease. *Biochemistry 57*, 4959−4962.



DOI: 10.1021/acs.biochem.9b00507
*Biochemistry* 2019, 58, 4505−4518